Quasiclassical Trajectory Study of Energy and Angular Distributions for the H + CO_2 → OH + CO Reaction†

Diego Troya, Matthew J. Lakin, and George C. Schatz*

Department of Chemistry, Northwestern University, 2145 Sheridan Road, Evanston, Illinois 60208-3113

Lawrence B. Harding

Chemistry Division, Argonne National Laboratory, Argonne, Illinois 60439-4803

Miguel González

Departament de Química Física i Centre de Recerca en Química Teòrica, Universitat de Barcelona, C/Martí i Franquès 1, 08028 Barcelona, Spain

Received: February 27, 2002; In Final Form: May 7, 2002

An extensive study of the H + CO_2 → OH + CO reaction dynamics has been carried out by means of the quasiclassical trajectory method employing three potential energy surfaces (PESs). The first PES corresponds to the earlier Bradley and Schatz (BS) surface. In the second PES (BSH), the BS surface was modified to include a new term that describes the OH + CO exit channel barrier and van der Waals region, based on high-level ab initio calculations. The third surface (LTSH) corresponds to a modification of the BSH surface where the energies of the various stationary points outside the exit channel region are calibrated from new ab initio calculations. We find that the correction in the exit channel improves the description of the energy partitioning to products, with both BSH and LTSH giving less release to translation and more to CO rotation than BS. These new results are in better agreement with measured product energy partitioning results, and we also find that the LSTH surface gives angular distributions that are in excellent agreement with experiment. Rovibrational state-resolved energy and angular distributions are also discussed. Details of the microscopic reaction mechanism are evaluated on the basis of an analysis of the dynamics as a function of the HOCO complex lifetime, leading to trends that provide insight on the complex-forming reaction fundamentals. In particular we find that the product internal distributions are independent of complex lifetime, while the angular distributions are strongly correlated with lifetime. The often used osculating complex model describes the angular distributions accurately for lifetimes shorter than half the rotational period but becomes inaccurate at longer times.

I. Introduction

The importance of the reaction H + CO_2 → OH + CO and its reverse in atmospheric and combustion chemistry has made this one of the most studied atom + triatom systems.[1] Many groups have examined this system, including extensive experimental and theoretical studies of the reaction dynamics. However, despite these conspicuous efforts, significant questions remain, thus providing motivation for additional studies. From a theoretical perspective, there are several limitations that have thus far precluded a thorough knowledge of the system. The ground-state potential energy surface is rather complex, exhibiting several stationary points and multiple reaction paths. This poses severe challenges to the development of a full-dimensional analytical potential energy surface. Regarding dynamics methodologies, the presence of a relatively deep minimum in the dominant minimum-energy reaction path enormously increases the size of the basis sets needed to describe the reaction dynamics by accurate quantum techniques. This, in addition to the fact that there is only one hydrogen atom involved, has inhibited accurate full-dimensional calculations of cross sections or rate constants. Only very recently[2] have full-dimensional calculations of the reaction probability restricted to zero total angular momentum become possible for the exothermic reverse reaction. There is also uncertainty about the possible role of nonadiabatic effects, as excited states are likely accessible to reaction for certain initial conditions.

From the experimental point of view, this system has been extensively studied over the years. Early important experiments were done under bulk conditions or with cleavage of van der Waals weakly bonded complexes to generate oriented reagents.[3] As a result, OH internal state distributions were determined under a wide variety of translational energies and always involving thermal CO_2.[4,5] The rovibrational distributions of the more rarely observed partner product CO have also been measured at 2.4 eV translational energy.[6,7] Recently, product translational energy distributions have also been determined by using polarized Doppler-resolved laser-induced fluorescence to specific rotational states of the product OH.[8,9] These sets of experiments have yielded OH state-resolved angular distributions,[8,9] along with information about the rotational polarization of the measured OH product.[10]

At the theoretical level, there has been significant interest in H + CO_2 and its reverse. The first extensive ab initio

† Part of the special issue "John C. Tully Festschrift".

* Corresponding author: e-mail schatz@chem.nwu.edu.

10.1021/jp0256950 CCC: $22.00
Published on Web 07/10/2002

calculations were used to derive a global analytical potential energy surface (PES) suitable for dynamics studies.[11] This first surface was later modified to improve the description of several stationary points,[12] and detailed quasiclassical trajectory (QCT) calculations were performed to compare with experiments.[13] Further improvements to this surface were done recently by Bradley and Schatz,[14] after which the stereodynamics properties of the reaction were compared with the experiments available at that time.[8a] However, all of the improvements added to the analytical surface were based on the early ab initio calculations by Schatz et al.[11] Recently, high-level ab initio calculations of the stationary points have been carried out by different groups. G2 and G2M quantum mechanics methods were used by Zhu et al. to calculate the system stationary points.[15] Duncan and Miller[16] employed the G3 model with complete basis set extrapolation to calculate the six stationary points involved in the minimum energy reaction path. Yu et al.[17] have calculated all of the stationary points of the ground-state surface using a coupled cluster method, also with complete basis set extrapolation. We are not aware of any dynamical calculations other than transition-state theory rate constants developed with these surfaces; however, the differences between the recent ab initio results and the earlier global fits used for dynamics studies are large enough that new dynamics studies are essential.

Recently, Harding and co-workers[18] have performed extensive high-quality (CCSD(T)/AUG-cc-pVDZ) ab initio calculations for parts of the HOCO ground- and excited-state potential surfaces, especially the region associated with the van der Waals interaction between OH and CO. Their results shed light on the details of the OH−CO weakly bound complex that corresponds to the product channel region of the $H + CO_2 \rightarrow OH + CO$ reaction. Motivated by the availability of the new ab initio data, it is the goal of this work to combine these data with the earlier global PES of Bradley and Schatz[14] to develop an improved surface for study of the $H + CO_2$ reaction dynamics. In addition, we will modify the BS potential to be consistent with recent ab initio estimates of the stationary points, and we refine the functional representation of BS so that energy conservation is improved in the QCT calculations.

We will verify the effects of these improvements to the HOCO surface by carrying out QCT calculations and comparing with the previous and recently reported experimental data available for $H + CO_2$ collisions. In addition, we will study interesting dynamics properties that have been left out in previous theoretical studies of this reaction due to energy conservation problems. These include the determination of both scalar and vector dynamics properties of the system as a function of the reaction complex lifetime. This will provide insight on the dynamics of complex-forming reactions, which have been, in general, less studied than direct reactions from a theoretical standpoint.

The paper is structured as follows: Section II gives details of the analytical potential energy surfaces employed in this work along with computational details of the dynamics calculations. Section III presents the dynamics study, and Section IV provides a brief summary and conclusions.

II. Potential Energy Surfaces and Computational Details

A. Potential Energy Surfaces. The basic features of the HOCO global potential energy surface are well-known, and a descriptive diagram of the energy as a function of the reaction coordinate can be found in earlier papers (see, for instance, Figure 1 of ref 14). The title reaction ($\Delta H_0^0 = 24.5$ kcal mol^{-1}) presents two dominant reaction pathways:

$$H + CO_2 \rightarrow \text{cis-HOCO} \rightarrow \text{trans-HOCO} \rightarrow OH + CO \quad (1)$$

$$H + CO_2 \rightarrow \text{HCO2} \rightarrow \text{trans-HOCO} \rightarrow OH + CO \quad (2)$$

where reaction sequence 1 corresponds to the minimum-energy reaction path.

We have employed three analytical potential energy surfaces in this study. The first is the surface of Bradley and Schatz (that we denote BS PES hereafter).[14] As mentioned above, this surface was derived from the first global analytical PES available from this system[11] by including several modifications to improve the characteristics of several stationary points. In this work we have modified the region of the OH + CO exit channel and OH−CO weakly bonded complexes by including an analytical (spline) function that interpolates a grid of ab initio points calculated following the work of Harding and co-workers.[18] The grid of points is calculated for a limited region of the reaction space and the remaining regions of the surface are represented by the BS PES (yielding a surface that we denote BSH hereafter). The switch between the BS PES and the function that interpolates the new ab initio calculations is done on the basis of the product OH internuclear distance (rOH) and on the distance between the OH and CO centers of mass (R). Thus, two hyperbolic tangent functions centered on $r\text{OH} = 2.6$ au and $R = 4.4$ au switch from the BS surface to the BSH surface whenever rOH and R are smaller and larger than these values, respectively. This ensures that the spline representation of the ab initio points is only called in the exit channel to OH + CO.

The procedure for deriving a six-dimensional expression in the OH + CO exit channel based on the ab initio grid of points is analogous to the strategy adopted in earlier QCT calculations of energy transfer in the reverse OH + CO reaction[19] and, more recently, to derive the WSLFH PES for the $H + H_2O \leftrightarrow H_2 + OH$ reaction.[20] There are three active coordinates that are the ones sampled in the ab initio grid of points, and the remaining three coordinates are regarded as inactive but are still included. These inactive coordinates are parametrized on the basis of semiempirical functions, whereas a spline interpolation is used for the active coordinates.

The electronic structure calculations reported here employ the open-shell spin-unrestricted coupled cluster theory, CCSD(T), of Knowles et al.,[21] which is generally regarded as the most accurate single-reference ab initio method currently available. The majority of calculations employ the augmented, correlation-consistent polarized double-ζ basis set (AUG-cc-pVDZ) of Dunning and co-workers.[22−24] All calculations were carried out with the MOLPRO package of codes.[25] The properties of the various long-range stationary points on this surface have been presented previously.[18] Here we describe only the analytic fit of the long-range interaction potential that will be used in the global potential surfaces described below. Calculations were done only for planar geometries and only for fixed OH and CO distances. The three active coordinates varied in these calculations are consistently defined following earlier work on this region of the surface.[19] These are (1) the distance between the centers of mass of the OH and CO (R), (2) the angle between the OH bond and the axis connecting to two centers of mass (θ_{OH}), and (3) the angle between the CO bond and the centers of mass axis (θ_{CO}). Signs are associated with both angles with the convention that geometries in which the C and the H are on the same side of the centers of mass axis are denoted with angles of the same sign, while geometries in which the C and

the H are on opposite sides are denoted with angles of opposite sign. The distance coordinate was varied from 3.3 to 20 au and the angles were sampled at 30° intervals. This yields a 23 × 13 × 13 rectangular grid, about half of which involves symmetry-unique points. Coupled-cluster calculations were carried out at all of the symmetry-unique points and the energies were then fit with a three-dimensional spline[26] to yield the final analytic function.

The three inactive coordinates are the internuclear distances of OH (rOH) and CO (rCO) and the dihedral angle between the planes defined by rOH and R and by rCO and R, which we denote θ_{HOCO}. Standard semiempirical Morse oscillator functions parametrize the rOH and rCO coordinates, whereas we have used a cosine function to parametrize the potential depending on the θ_{HOCO} variable:

$$V(\theta_{HOCO}) = \frac{1}{2}[V(\theta_{HOCO} = 0)(1 + \cos\theta_{HOCO}) + V(\theta_{HOCO} = \pi)(1 - \cos\theta_{HOCO})]$$

This function provides a smooth connection between the two planar HOCO configurations $\theta_{HOCO} = 0$ and $\theta_{HOCO} = \pi$ that is in excellent agreement with sample nonplanar CCSD(T)/AUG-cc-pVDZ ab initio predictions in that region of the surface.

Hence the total potential energy in that region is the sum of the contributions of the potential due to the active variables, V_a, and the inactive variables, V_i: $V = V_a + V_i$, where V_i is

$$V_i = V_{Morse,OH} + V_{Morse,CO} + V(\theta_{HOCO})$$

The third surface employed in this work corresponds to a modification of the energies of the stationary points outside the OH−CO exit channel on the BSH surface according to the recent high-level ab initio calculations by Duncan and Miller[16] and Yu et al.[17] We will give the details of this new surface elsewhere;[27] however, we should mention the major changes that have been made in the energy of the stationary points. The entrance barrier to the HOCO minimum from the H + CO_2 asymptote has been lowered substantially. This barrier is 3.0 kcal mol^{-1} above the OH + CO asymptote in the BS PES (placed 22.3 kcal mol^{-1} above H + CO_2), and about 1.5 kcal mol^{-1} above OH + CO in the new surface, in agreement with the calculations of Yu et al.[17] The other significant modification concerns an improvement in the HCO_2 well depth. Whereas in the BS PES this minimum has an energy of about 2.5 kcal mol^{-1} below the H + CO_2 asymptote, new ab initio calculations[17] show that this minimum is around 9 kcal mol^{-1} above this asymptote. In the new analytical surface that we have derived in this work, the HCO_2 minimum is placed 7.8 kcal mol^{-1} above H + CO_2. Minor changes have also been made to the remaining stationary points in order to best match the energies predicted by these high-level ab initio calculations. We omit these less important details here and kindly refer the reader to a forthcoming paper.[27] We shall henceforth denote this surface as LTSH.

Other improvements included in both the BSH and LTSH surfaces refer to the nature of the functions used to describe certain features of the analytical PES. We observed that the BS PES exhibited singularities in the energy derivatives used in the QCT calculations for geometries where three of the four atoms are close to being collinear. These singularities give rise to problems with energy conservation that inhibit the evaluation of certain cross sections, especially those that involve relatively long duration trajectories. In developing the BSH and LTSH PES we have devoted substantial effort to smoothing out these singularities. As a result, trajectory calculations are more stable and energy conservation criteria can be tighter than for BS. The BS surface, however, has not been smoothed so that we can make comparison with previous published results. This means that the problems with energy conservation are still present in BS, and because of this we will only present limited results for this surface (emphasizing results that are less sensitive to energy conservation problems).

Summarizing, we employ three different potential energy surfaces. The first is the BS PES. The second is the BSH PES, a surface with a smooth energy functional and a new term for the exit channel leading to OH + CO but with the same energies as BS for the rest of stationary points. LTSH is also smooth and contains the new term for the exit channel, but the energies of the rest of the stationary points have been calibrated based on very recent ab initio estimates.

B. Computational Details. The equations of motion were solved by the QCT method for atom + triatom reactions as described in our previous work.[28−31] The basic difference between this code and standard QCT algorithms lies in the selection of the triatomic internal states by means of a semiclassical action calculation, which has been explained elsewhere.[32,33] All of the calculations carried out in this work involve CO_2 in its ground vibrational state. While the action method is specifically designed to prepare vibrationally excited triatoms, we have used it in this work since it also allows us to specify rotation. The rotational state of CO_2 has been fixed at $J = 15$, which is the most populated rotational state at room temperature. Comparison with experiments that resolve OH rotational states requires an abnormally large computational effort. Batches of 1 million trajectories/surface and translational energy have been calculated in order to have enough reactive trajectories in the OH rotational states for which there exists experimental information. A total of 12 million trajectories have been calculated in this work.

The integration step has been fixed at 10 au. However, it should be noted that total energy is not as perfectly conserved throughout the evolution from reagents to products as in our earlier studies of other atom + triatom systems.[28−31] A smaller integration step does not improve energy conservation in the trajectories since the system dynamics (with the presence of several deep minima) make it more difficult to conserve total energy with longer trajectories. Although the revised functional representation of the potential substantially improves energy conservation, the energy conservation requirements have to be still somewhat more relaxed in comparison to what is normally required for atom + triatom direct reactions.[30,31] In particular, 1% energy conservation relative to the reagent total energy is enforced for BSH and LTSH surfaces. This relatively large criterion implies about 200 cm^{-1} uncertainty in product energy for the largest translational energy considered (2.5 eV), which is larger than the spacing between OH rotational levels below $j = 5$ and between almost all of the CO rotational levels that are populated. To test the importance of this, we have done additional calculations in which energy conservation to within 0.2% is required, corresponding to an uncertainty in energy that is smaller than the OH rotational spacing and smaller than the CO spacing for j smaller than 10. Analysis of energy partitioning and angular distribution information with this more stringent energy conservation condition reveals that there is essentially no change in averaged properties. Since the more relaxed energy conservation condition gives smaller statistical uncertainties in the results (as fewer trajectories are rejected), we shall use this in all the results we present. We have also checked total angular momentum conservation, and we find that this is better

conserved than total energy, typically to five or six figures for the trajectories that satisfy the energy conservation condition.

Trajectories are started at an initial reagent separation of $12a_0$ and are stopped at the same product separation. Caution is used in defining the product separation in the diatom + diatom channel due to the presence of weak van der Waals complexes in that region of the surface. In the exit channel on the new surfaces, the HO−CO minimum is located at about $R = 7.5a_0$, and the asymptotic energy is reached at about $R = 9.5a_0$.[18] Therefore, $12a_0$ is a distance long enough to avoid long-range interactions between nascent products. The validity of these values has been verified by use of longer reagent or product distances such as $15-20a_0$. The maximum impact parameter (b_{max}) was allowed to depend on initial translational energy, with b_{max} set equal to $4.5a_0$ for $E_T = 2.3$ eV and above and to $4.2a_0$ for lower collisional energies. In previous atom + triatom calculations,[28,30,31] the inclusion of zero-point constraints was found to be important in optimizing the agreement between quantum and QCT excitation functions close to threshold. For example, for the H + H_2O reaction, it was found[34] that requiring the newly formed diatom to have at least zero-point energy led to reasonable agreement between classical and quantum integral cross sections. However, for this same reaction,[30,31] application of this ad hoc procedure (i.e., constraining the H_2 zero-point energy) to study the H_2 internal distributions gave ambiguous results. Thus the constraint was found suitable for simulating the internal state distributions reported by the Zare group,[35] but not requiring the zero-point energy did a better job in matching a different set of experiments by Brouard and co-workers.[36] In view of this ambiguity, and also realizing that the title reaction proceeds via intermediate complex formation while the earlier reactions were all direct reactions, we present below a study of the effect of the various possible choices in the treatment of zero-point energy. We will show that unconstrained results give the physically most reasonable results, so the bulk of our results refer to unconstrained calculations.

In this work we shall focus in part on how the lifetime of the reaction complex influences the reaction dynamics. It is therefore necessary to define the complex lifetime, so in this work we will start and stop the complex lifetime clock based on internuclear distances. The reaction complex is defined as having formed whenever an H−O distance or the H−C distance is smaller than the corresponding entrance channel saddle point distance for the first time (rOH of H + CO_2 → *cis*-HOCO saddle point = $2.91a_0$; rCH of H + CO_2 → HCO_2 saddle point = $3.82a_0$). Likewise, the clock is stopped when the separation between the nascent diatomics corresponds to the saddle point distance associated with the spline-fitted ab initio points that we use in this work to represent the OH + CO exit channel in the BSH or LTSH ($R = 4.8a_0$). Although there are more accurate ways to define a complex lifetime, for instance on the basis of turning points,[37] we believe that this definition is reasonable enough given the goal of this study.

III. Dynamics

A. Product Energy Partitioning. Table 1 presents cross sections and product energy disposal results as a function of translational energy (and without zero-point constraints). This shows that the BSH and LTSH surfaces give similar values for cross sections but with different dependence on energy. Whereas the BSH excitation function seems to reach a maximum at $E_T = 2.09$ eV, the LTSH cross sections decrease monotonically with increasing energy. Calculations at lower energies for the LTSH PES reveal that there is no reactivity at $E_T = 1.0$ eV, and between $E_T = 1.15-1.86$ eV the cross section increases rapidly [$\sigma = (0.05 \pm 0.01)a_0^2$, $(0.30 \pm 0.01)a_0^2$, and $(0.72 \pm 0.02)a_0^2$ at $E_T = 1.15$, 1.36, and 1.64 eV, respectively]. This gives the expected shape of an excitation function for reaction over a barrier, with a steep increase in the cross section right above the threshold, peak reactivity at about $E_T = 1.86$ eV, and then a decreasing cross section at higher energies. The same shape is observed for the BSH PES, except that the peak is located at higher translational energies and the cross section decays more slowly as energy is increased.

TABLE 1: Cross Section and Energy Disposal as a Function of Translational Energy[a]

	BS	BSH	LTSH
		1.86 eV	
σ/a_0^2		0.68 ± 0.01	0.78 ± 0.01
b_{max}/a_0	3.74	3.75	3.93
$\langle v_{OH} \rangle$	0.08	0.11	0.11
$\langle v_{CO} \rangle$	0.26	0.33	0.33
f'_T	0.60	0.48	0.48
$f'_{VIB}(OH)$	0.04	0.05	0.05
$f'_{ROT}(OH)$	0.17	0.20	0.20
$f'_{VIB}(CO)$	0.07	0.09	0.09
$f'_{ROT}(CO)$	0.12	0.18	0.18
		2.09 eV	
σ/a_0^2		0.73 ± 0.01	0.74 ± 0.01
b_{max}/a_0	3.79	3.84	4.06
$\langle v_{OH} \rangle$	0.20	0.18	0.18
$\langle v_{CO} \rangle$	0.45	0.47	0.48
f'_T	0.54	0.46	0.46
$f'_{VIB}(OH)$	0.07	0.07	0.07
$f'_{ROT}(OH)$	0.16	0.20	0.20
$f'_{VIB}(CO)$	0.10	0.10	0.10
$f'_{ROT}(CO)$	0.13	0.17	0.17
		2.30 eV	
σ/a_0^2		0.70 ± 0.01	0.64 ± 0.01
b_{max}/a_0	3.92	3.95	4.10
$\langle v_{OH} \rangle$	0.29	0.26	0.26
$\langle v_{CO} \rangle$	0.60	0.60	0.60
f'_T	0.50	0.44	0.44
$f'_{VIB}(OH)$	0.09	0.08	0.08
$f'_{ROT}(OH)$	0.18	0.20	0.20
$f'_{VIB}(CO)$	0.11	0.11	0.11
$f'_{ROT}(CO)$	0.12	0.17	0.17
		2.50 eV	
σ/a_0^2		0.66 ± 0.01	0.55 ± 0.01
b_{max}/a_0	3.96	4.07	4.13
$\langle v_{OH} \rangle$	0.32	0.36	0.33
$\langle v_{CO} \rangle$	0.67	0.71	0.73
f'_T	0.50	0.42	0.42
$f'_{VIB}(OH)$	0.09	0.10	0.09
$f'_{ROT}(OH)$	0.19	0.20	0.21
$f'_{VIB}(CO)$	0.11	0.12	0.12
$f'_{ROT}(CO)$	0.11	0.16	0.16

[a] Both average vibrational numbers and fractions of energy have an error bar lower than ±0.01.

In Table 1 and Figure 1 we show the fraction of energy in vibration and rotation of each diatomic as a function of the relative translational energy for the BS, BSH, and LTSH surfaces. We see that the energy partitioning is not statistical (in the statistical limit, the vibrational and rotational fractions of both diatomics would be nearly identical). This suggests that although progress from reactants to products involves the formation of an intermediate complex, the complex lifetime is not long enough to allow for randomization of the internal energy. This trend has been known for this reaction since the early trajectory studies of H + CO_2. We also see that half of the available energy ends up in translation and that this decreases as reagent translational energy increases (Figure 1a). The

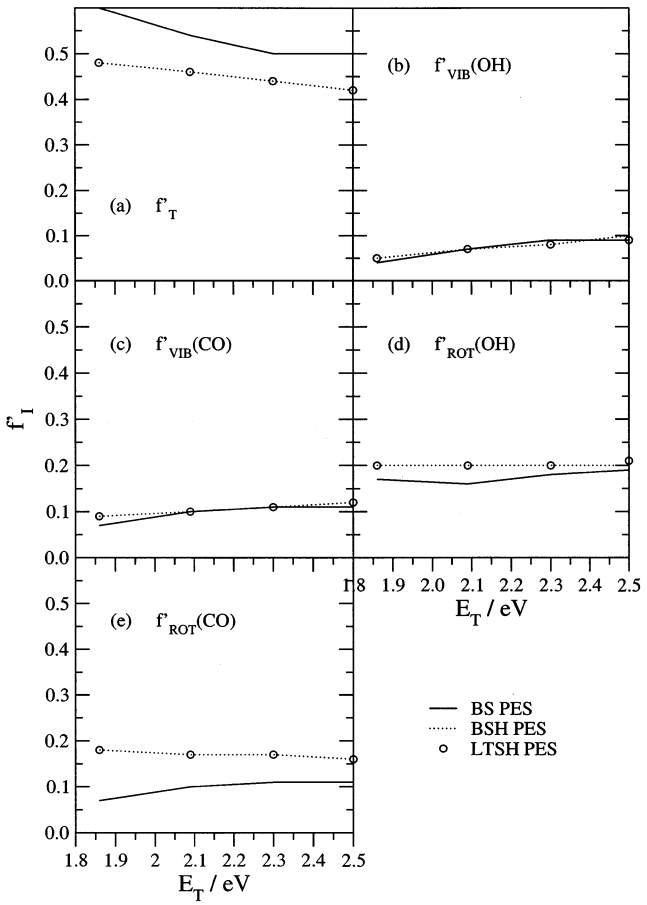

Figure 1. QCT product energy disposal expressed in terms of energy fractions as a function of translational energy for the H + CO_2 → OH + CO reaction with the three surfaces employed in this study: (a) f'_T; (b) f'_{VIB}(OH); (c) f'_{VIB}(CO); (d) f'_{ROT}(OH); (e) f'_{ROT}(CO). Error bars lower than ±0.01 are omitted for clarity.

average fraction in OH vibrational energy increases with E_T (Figure 1b), whereas this increase is slower for CO vibration (Figure 1c). OH rotational energy increases at the same rate as the available energy does, so that the average fraction of energy released to this mode remains constant with E_T (Figure 1d). The increase of CO rotational energy is even slower with E_T, and the average fraction of CO rotational energy [f'_{ROT}(CO)] slightly decreases with increasing E_T for BSH and LTSH PES (Figure 1e).

The BS PES shows noticeable differences from either the BSH or the LTSH PES, both of which incorporate the new exit channel potential derived from high-level ab initio calculations. In particular, the release of energy to CO rotation in BSH and LTSH is greater than in BS, and product translational excitation is smaller. The energy partitioning for the remaining modes is approximately equal for all of the surfaces. Thus the addition of the new potential calculated from an ab initio grid of points around the OH + CO exit channel promotes CO rotational excitation at the expense of product translation.

To understand the effect of the exit channel region on the energy partitioning, we plot in Figure 2 contours of relevant portions of the BS and BSH PES. The graphs are presented in a format that follows the earlier work of Harding and coworkers.[18] The plots represent the potential energy surface in a molecule fixed Cartesian coordinate system. The origin of coordinates is the CO center of mass, and CO is aligned along *x* with C pointing toward the positive *x* direction. Each point refers to (R, θ_{CO}) values that have been converted to Cartesian coordinates. θ_{OH} is optimized for each point, and the system is in a planar (minimum-energy) configuration. Top panels are for BS (left) and BSH (right) surfaces with fixed rOH = 1.83a_0 and rCO = 2.13a_0 distances. These interatomic distances roughly correspond to the diatomic equilibrium distances. Bottom panels represent the same plots but with rCO = 2.30a_0. This value of rCO roughly corresponds to the outer turning point of the CO(v = 1) state. As we shall see below, a large fraction of trajectories ends up with the CO vibrationally excited, so the bottom panels are useful for studying regions other than the minimum-energy one that are important to the reaction dynamics. We see in the figure that the differences between BS (left panels) and BSH (right panels) are substantial. The HOCO well shows up as a relatively large hole near the carbon atom in the BS surface and a much smaller hole for BSH, although deeper. The saddle point for decay of HOCO to OH + CO is closer to having OCO collinear on BS than on BSH, and the reaction path is narrower on BSH. The differences between BS and BSH are all exaggerated for rCO = 2.30a_0, with the barrier disappearing entirely on BS. The narrower reaction path and more bent transition state on the BSH surface will likely produce stronger torques on the CO molecule, resulting in larger CO rotational excitation, as observed.

The fact that there is negligible difference between the BSH and the LTSH energy partitioning data, with average fractions of energy in products overlapping at all energies calculated, is also notable. This means that the energy is released in locations that are common to both surfaces. Since the only region completely identical for both surfaces involves the reaction path leading to OH + CO formation, i.e., the part of the surface defined in terms of the spline function, we conclude that the topology of the surface around this reaction path is dominant in determining energy partitioning. The fact that only translation and CO rotational energy are changed in comparing BS with the other two surfaces indicates that the energy release behavior for the remaining degrees of freedom must be similar.

Another difference between BS and BSH is the occurrence of van der Waals wells on BSH for both OCHO and OHCO linear configurations. Indeed, the reaction path for dissociation of HOCO to OH + CO passes through the linear OCHO minimum on the way to OH + CO. However, given the high-energy conditions involved in the study, the system is not likely to follow the minimum-energy reaction path in the van der Waals region. To study this point, we have performed additional QCT calculations at 2.5 eV on a surface that is identical to LTSH except that van der Waals wells have been removed, and the potential is simply flat for OH + CO separations that are much outside the barrier. We find that the resulting energy partitioning results are numerically identical to what we present in Table 1 at this energy, indicating that the van der Waals well has no influence on product energy partitioning at this energy.

The analysis to this point has demonstrated that the modifications made to the BS surface lead to important effects on energy partitioning behavior. Now we would like to see if this effect leads to an improvement in the comparison with available experiments.

A complete picture of the product energy partitioning has been difficult to determine from the various measurements. Jacobs et al.[5c] reported for E_T = 1.86 eV that f'_T = 0.43, f'_{VIB}(OH) = 0.03, and f'_{ROT}(OH) = 0.13, and by energy difference they estimated f'_{INT}(CO) = 0.41. Our calculations on the LTSH PES are able to satisfactorily reproduce the release to translation (f'_T = 0.48), an important improvement on the BS result (f'_T = 0.60). Vibrational excitation of OH is in

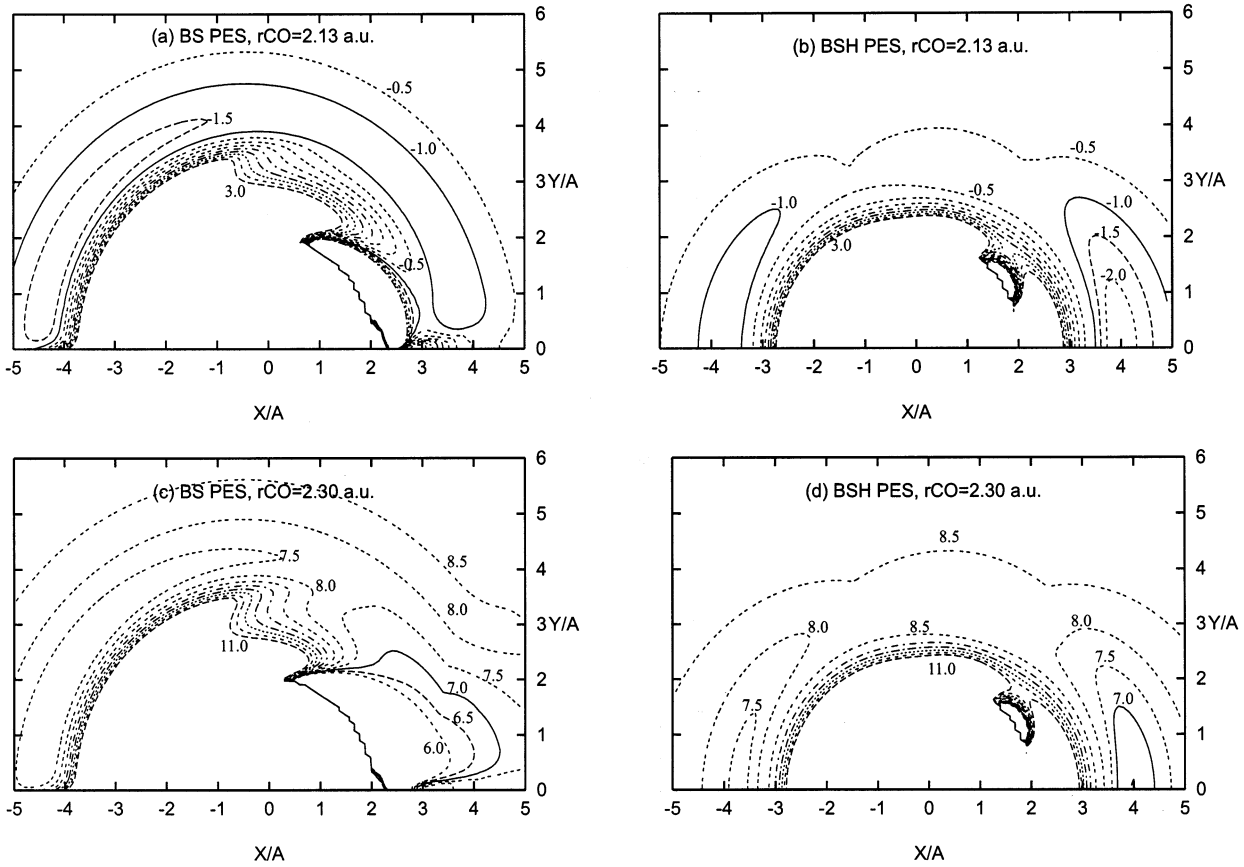

Figure 2. Contour energy diagrams for the BS and BSH surfaces exit channel: (a) BS surface for rCO = 2.13a_0; (b) BSH surface for rCO = 2.13a_0; (c) BS surface for rCO = 2.30a_0; (d) BSH surface for rCO = 2.30a_0. The labels are energies in kilocalories per mole with respect to the OH + CO asymptote. Contours are plotted each 0.5 kcal mol^{-1}. Lengths are given in angstroms. See text for details.

agreement with experiment for all surfaces, but OH rotational excitation is a bit high. CO excitation is lower than experiment for BS, but the above-mentioned enhancement of CO rotational excitation on the new surfaces makes the calculated CO internal excitation closer to the experimental estimates.

The availability of experimental data enables us to consider the effect of the different choices of zero-point energy constraints on the comparison with experiment. Here we only consider the LTSH surface. If we consider constraining just OH, we find that this leads to a hotter OH vibrational distribution than in the unconstrained results, with $f'_{VIB}(OH) = 0.14$. Energy release to all of the other modes is diminished with this constraint [$f'_T = 0.44$, $f'_{ROT}(OH) = 0.19$, $f'_{VIB}(CO) = 0.06$, $f'_{ROT}(CO) = 0.17$]. Comparison with the experimental results described above shows that f'_{VIB} is about 5 times the measured fraction, indicating that this form of zero-point constraint is inadequate for H + CO_2. Constraining CO vibration (and not OH vibration) leads to CO vibrational distributions that are hotter than in the unconstrained calculations, with smaller energy release to the other degrees of freedom [$f'_T = 0.45$, $f'_{VIB}(OH) = 0.03$, $f'_{ROT}(OH) = 0.19$, $f'_{VIB}(CO) = 0.16$, $f'_{ROT}(CO) = 0.17$]. This makes the calculated results closer to the experiments described above. Constraining zero-point energy of both nascent diatoms leads again to overexcited OH vibration [$f'_T = 0.42$, $f'_{VIB}(OH) = 0.11$, $f'_{ROT}(OH) = 0.17$, $f'_{VIB}(CO) = 0.14$, $f'_{ROT}(CO) = 0.16$]. Thus on the basis of these results it could be stated that the procedure that best matches experiment is to constrain the diatomic whose bond is not formed in the reactive process to have at least zero-point energy. This is at odds with what was used for H + H_2O, where the constrained bond is the one formed in the reactive process.

Additional insight into the theory/experiment comparison is provided by considering Wolfrum group results at 2.3 eV, which show $f'_T = 0.59 \pm 0.16$, $f'_{VIB}(OH) = 0.11 \pm 0.02$, and $f'_{ROT}(OH) = 0.14 \pm 0.02$, and thus $f'_{INT}(CO) = 0.16$ by energy difference.[5d] Our unconstrained calculation of energy release to translation lies within the large experimental uncertainty for all surfaces, although BS is somewhat closer than the newer surfaces. Energy channeling to OH vibration is also satisfatorily reproduced by all surfaces, and OH rotation seems again to be slightly too high in the calculations. Constraining the OH zero-point energy at this energy gives (with LTSH) $f'_T = 0.41$, $f'_{VIB}(OH) = 0.16$, $f'_{ROT}(OH) = 0.18$, $f'_{VIB}(CO) = 0.09$, and $f'_{ROT}(CO) = 0.16$. For constrained CO we find $f'_T = 0.41$ $f'_{VIB}(OH) = 0.07$, $f'_{ROT}(OH) = 0.19$, $f'_{VIB}(CO) = 0.17$, and $f'_{ROT}(CO) = 0.16$. Constraints in both diatomics give $f'_T = 0.38$, $f'_{VIB}(OH) = 0.15$, $f'_{ROT}(OH) = 0.17$, $f'_{VIB}(CO) = 0.15$, and $f'_{ROT}(CO) = 0.15$. Here we see that constraining the OH reduces the CO internal energy release, making it closer to experiment, but at the same time giving overexcited OH and lower release to translation compared with experiment. Constraints on CO or on both OH and CO make the CO energy release larger than experiment and diminish the release to translation. According to these results, the absence of any constaints is the best procedure to match experiment. Due to the lack of accord between these findings and what was discussed above at 1.86 eV, we report only unconstrained results hereafter.

The CO internal state distributions were directly measured by two different groups[6,7] using a rather close translational energy (E_T = 2.4 eV). However, there were remarkable discrepancies between the results from the two experiments.

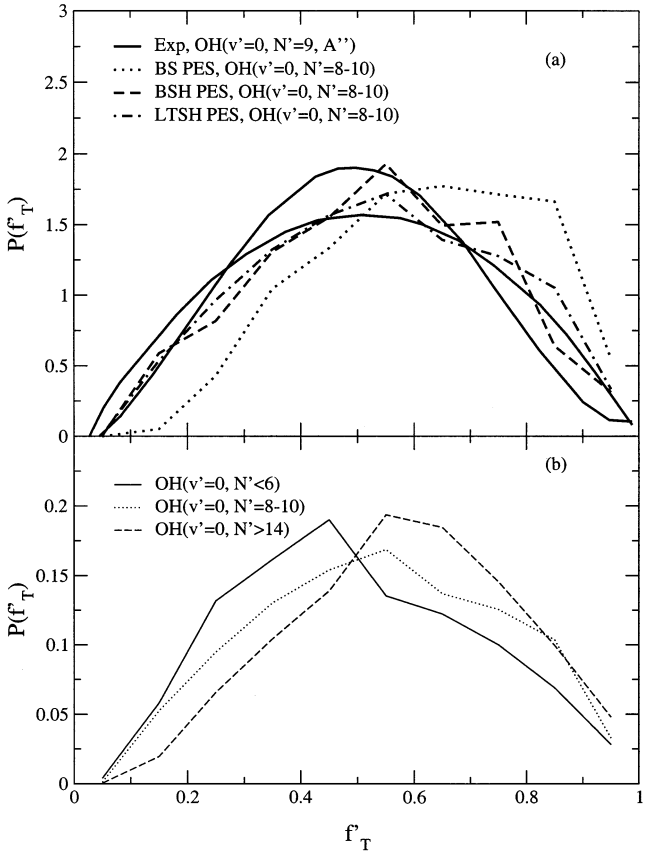

Figure 3. (a) Experimental and QCT kinetic energy release for the H + CO_2 → CO + OH(v' = 0, N' = 9) reaction at E_T = 2.5 eV. Experiments are from ref 9. The narrower distribution corresponds to the s = 1/2 spin−orbit state and the broader distribution to the s = 3/2 spin−orbit state. (b) QCT kinetic energy release for the H + CO_2 → OH(v' = 0, N') + CO reaction at E_T = 2.5 eV as a function of OH rotational excitation and employing the LTSH PES.

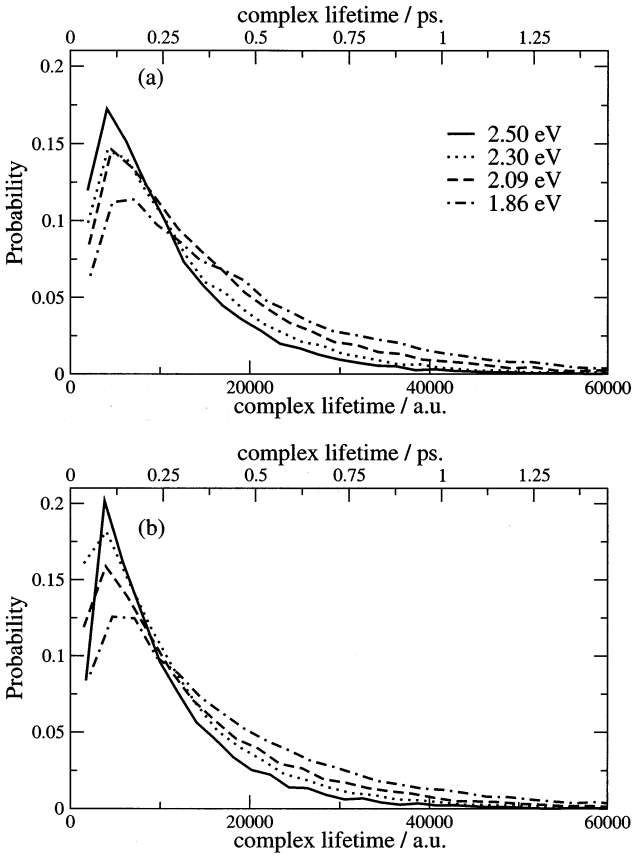

Figure 4. QCT collision complex lifetime as a function of reagent's translational energy for the H + CO_2 → OH + CO reaction: (a) BSH PES; (b) LTSH PES.

Rice and Baronavski[6] reported a CO vibrational ratio of $P(v' = 1)/P(v' = 0) = 1$, whereas Wittig and co-workers[7] reported a smaller ratio (0.4). Our QCT calculations seem to be closer to Wittig's results (0.57 on BS, 0.47 on BSH, and 0.50 on the LTSH PES). Rotational distributions were thought to be relaxed in the experiments of Wittig and co-workers. However, Rice and Baronavski reported that the average CO rotational state in CO($v' = 0$) was $\langle J_{v'=0}\rangle = 13$, and $\langle J_{v'=1}\rangle = 20$ for CO($v' = 1$). Our data on BS are $\langle J_{v'=0}\rangle = 24$ and $\langle J_{v'=1}\rangle = 23$, and $\langle J_{v'=0}\rangle = 30(29)$, $\langle J_{v'=1}\rangle = 29(27)$ on BSH(LTSH). The first noticeable issue from these results is that, unlike the experiments, we do not see a positive correlation between vibration and rotation in CO (i.e., higher rotational excitation for higher vibrational excitation). Indeed, such a strong positive correlation has never been seen in any direct atom + diatom or atom + polyatom reaction, where the universal behavior is a negative correlation between vibration and rotation (i.e., less excited rotational distributions with increasing vibrational level). Very slight positive correlations have been found in H + CD_4 → HD + CD_3,[38] and H(Cl) + HCN → H_2(HCl) + CN,[28,29] where products arising in HD($v' = 1$) or CN($v' = 1$) have slightly higher rotational energy than those in the vibrational ground state.

OH product state-selected energy partitioning data are also available. Brouard et al. [9] have recently reported OH state-specific product translational energy distributions for a variety of rotational, spin−orbit, and Λ-doublet states of OH. Two different reagent translational energies were also considered in these experiments, E_T = 1.8 and 2.5 eV. Figure 3a shows the experimental fractions of product translational energy for the OH($v' = 0$, $N' = 9$) generated from the title reaction at E_T = 2.5 eV. Although the experimental measurements include other rotational states of OH (N' = 1, 5, 9, and 11 in $v' = 0$ and N' = 1 and 3 for $v' = 1$), we chose to establish comparisons with $N' = 9$ for several reasons. First, $N' = 9$ is close to the peak of the OH($v' = 0$) rotational distribution, so this is where more reactive trajectories are available for the theoretical analysis. Second, there is an important dependence of the results on Λ-doublet state for rotational states colder than $N' = 5$ that we cannot describe, so it is better to work with higher N' where the Λ-doublet state is not important. Moreover, measurements of the dependence of the kinetic energy release on OH spin−orbit state indicate very strong differences between the kinetic energy release for the two spin−orbit states of OH, particularly for rotationally cold OH. However, at $N' = 9$ the differences between spin−orbit states have mostly vanished. Unfortunately there are no complete measurements of this for $N' = 5$.

Figure 3 plots the translational distribution $P(f'_T)$ for selected states of OH. Here f'_T is defined as $f'_T = E'_T/[E'_T + E'_{INT}(CO)]$, or the ratio of the product translational energy to the total available energy for a given state of OH. Whereas the BS surface predicts more kinetic energy release (less excited CO) than is experimentally determined, both BSH and LTSH show better agreement with the experiments. This state-specific comparison, together with the global observations for E_T = 1.86 eV, demonstrates that BSH and LTSH are significantly improved over BS in determining product translational energy release. Figure 3b presents the kinetic energy release as a function of OH rotational state. Here we see that as the OH rotational state increases, there is a greater fraction of energy released to product translational energy. This implies that the CO rovibrational

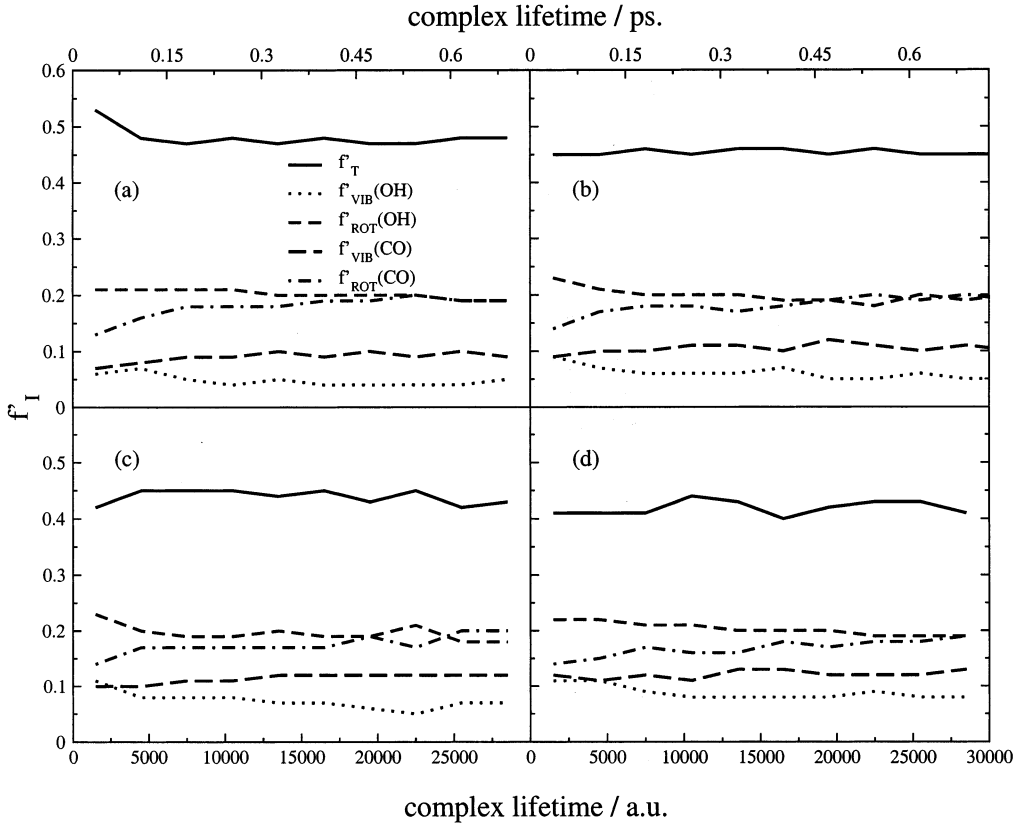

Figure 5. QCT average fractions of energy in products as a function of the collision complex lifetime for the H + CO_2 → OH + CO reaction employing the LTSH PES: (a) $E_T = 1.86$ eV; (b) $E_T = 2.09$ eV; (c) $E_T = 2.30$ eV; (d) $E_T = 2.50$ eV. —, Average fraction of product translational energy; ··· (— — —), average fraction of OH (CO) vibrational energy; --- (-·-), average fraction of OH (CO) rotational energy.

distributions are colder as the OH gets more excited, indicating that there is a competition between OH and CO internal modes in the product energy partitioning.

To gain greater insight on the dynamical mechanism controlling the title reaction, we have analyzed the distribution of product energy as a function of HOCO complex lifetime. The probability distribution of complex lifetimes for various collisional energies for the BSH PES are plotted in Figure 4a, and those belonging to the LTSH PES are in Figure 4b. We see that lower collision energies imply longer complex lifetimes, as expected. We also note that the BSH PES average lifetimes are longer than those for the LTSH PES by about 10%. This is consistent with the shallower HOCO well on LTSH, as dictated by revised estimates of the HOCO heat of formation.

Figure 5 shows the evolution of energy partitioning as a function of complex lifetime for E_T = (a) 1.86, (b) 2.09, (c) 2.30, and (d) 2.50 eV translational energies for the most relevant range of complex lifetimes on the LTSH PES. The surprising point that emerges from the figure is that the energy fractions are largely uncorrelated with complex lifetime. It is commonly thought that as the complex lifetime increases, energy has more opportunity to flow between modes. Therefore, longer-lived complexes should have an energy release closer to the statistical predictions. But what we see in Figure 5 is clearly at odds with this expected trend. The fractions are fairly constant irrespective of the time that the system has remained in the complex, and this is seen for all translational energies explored.

There are, however, some weak tendencies that should be noted in Figure 5. CO rotational excitation appears to increase with increasing complex lifetime. This energy increase primarily is coupled to a decrease in OH vibrational excitation. Thus we see that energy flows out of the newly formed OH bond while the complex ages and into a low-frequency internal mode of the HOCO complex that ultimately turns into CO rotation. Analysis of BS and BSH results supports this conclusion.

B. Angular Distributions. Study of angular distributions is particularly relevant for this system due to the presence of new experimental results by Brouard et al.[8,9] Figure 6 exhibits angular distributions for several choices of translational energy for the BSH (panel a) and the LTSH (panel b) surfaces. This figure shows distributions that are largely independent of collisional energy, with a notable bias toward forward scattering.

The measured angular distributions are for specific OH rotational levels, so here we again choose to compare with the OH($v' = 0, N' = 9$) results at $E_T = 2.5$ eV for the reasons mentioned above. Figure 7 depicts calculated results for the BSH and LTSH PES, together with the experimental results. These correspond to the two spin−orbit states of the Λ-doublet A″ state of OH. We see that there is excellent agreement between the calculated (LTSH) distribution with full rotational resolution in OH($v' = 0, N' = 9$) and the experiments. Like the global distributions described previously, the state-specific distributions are dominated by forward scattering. This is in clear agreement with experiments. The BSH result is similar but LTSH is clearly better.

Another property of interest in the experiments is the dependence of the angular distributions on product state. Figure 8 shows the QCT OH vibrational state-selected (panel a) and OH($v' = 0$) rotational state-selected (panel b) angular distributions for the title reaction at $E_T = 2.5$ eV and employing the LTSH surface derived in this work. From either plot we see only a very slight tendency toward less forward excitation with increasing OH vibrational and decreasing OH rotational excitation. This is somewhat at odds with what was claimed from

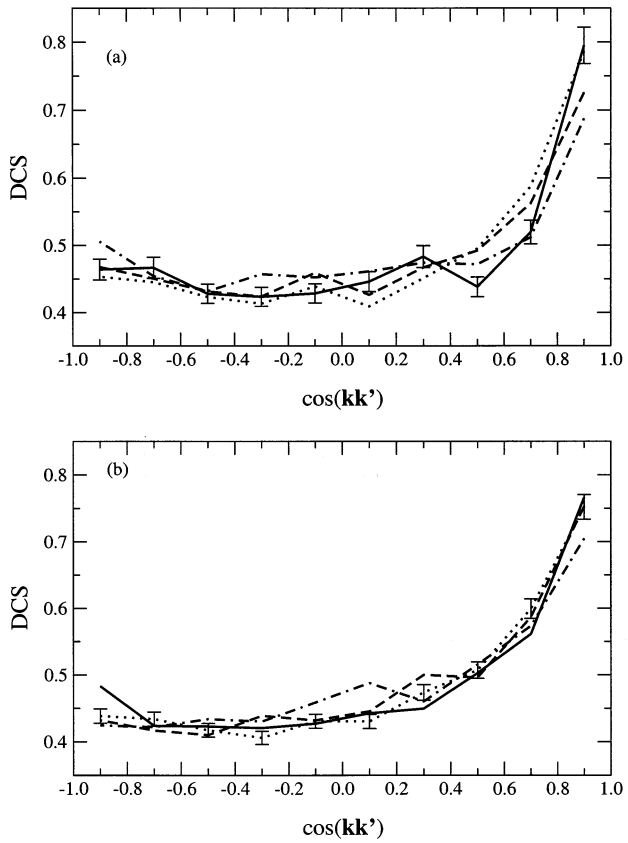

Figure 6. QCT angular distributions expressed in terms of normalized differential cross sections $[(2\pi/\sigma)(d\sigma/d\omega)]$ for the H + CO_2 → OH + CO reaction as a function of translational energy: (a) BSH PES; (b) LTSH PES. Energy legends are the same as in Figure 4.

the experiments,[9] where it was stated that the microscopic reaction pathways are under dynamical control, being sensitive to product quantum state.

There are several ways to rationalize the discrepancies between what was estimated from the experimental results and the theoretical predictions. Inaccuracies in the surface are always possible. Moreover, for this reaction, the adiabatic approximation has been questioned several times, and indeed, nonadiabaticity was claimed to be responsible for the different angular distributions seen for various states of OH.[9] Finally, the experimental determinations have a large degree of uncertainty and detect single spin−orbit and Λ-doublet OH states, which are not described at this level of theory.

Analysis of the complex lifetime-resolved angular distributions is thought to provide key information about the mechanisms that control the title reaction. Angular distributions for various collision complex lifetimes are plotted in Figure 9 at $E_T = 1.86$ eV for the LTSH PES. Figure 9a shows the results for collision complexes that live up to 15 000 au. The differences between different times within this interval are rather striking. It is clearly seen that the short-lived trajectories exhibit strong backward scattering, with almost zero differential cross section in the most forward scattering bin. As the lifetime increases we see a gradual shift toward less backward scattering, through isotropic scattering, to strong forward scattering at 13 500 au lifetime. Animation of trajectories reveals that in short-lived complexes when the H atom gets close enough to the CO_2 molecule, the HOCO complexes are formed very briefly, so no rotation of the complex can occur, and the OH product is scattered in the opposite direction to the incident H. If the collision complex is allowed to live longer, rotation of the complex is observed. The scattering is then influenced by rotation of the complex such that, if the lifetime allows for a half-turn of the complex, forward scattering is observed.

Figure 9b depicts the 15 000−30 000 au lifetime interval. Here we see that the angular distribution has its largest forward scattered maximum at 16 500 au (400 fs), corresponding to the most probable time for half a rotation of the HOCO complex. From there on we see a propensity toward less forward scattering

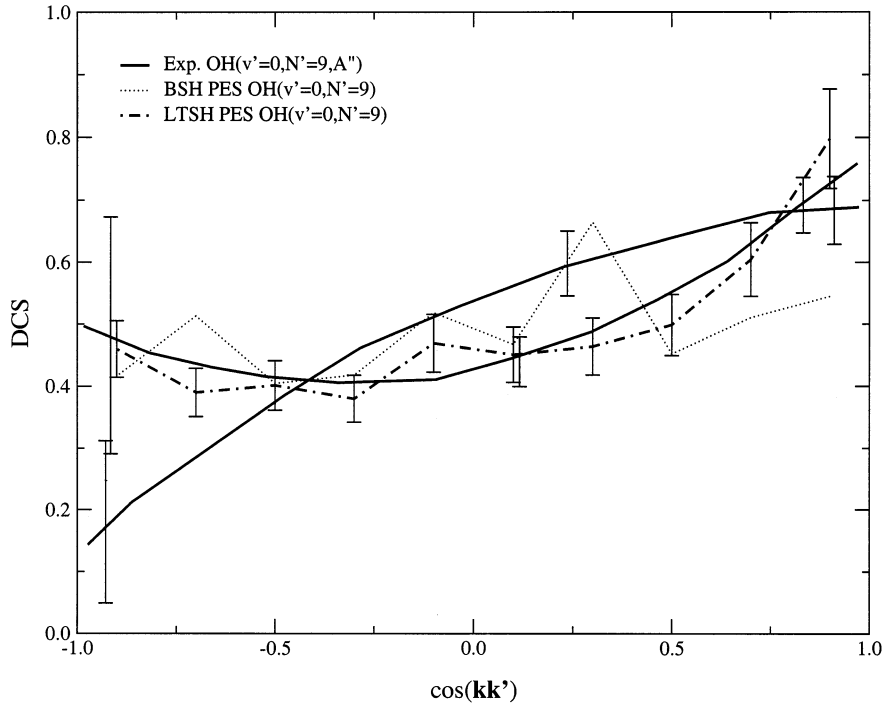

Figure 7. Experimental and theoretical QCT angular distributions expressed in terms of normalized differential cross sections $[(2\pi/\sigma)(d\sigma/d\omega)]$ for the H + CO_2 → OH($v' = 0$, $N' = 9$) + CO reaction at $E_T = 2.5$ eV. Concave experimental DCS is for the spin−orbit state $\Omega = 1/2$, whereas convex DCS is for $\Omega = 3/2$.[9]

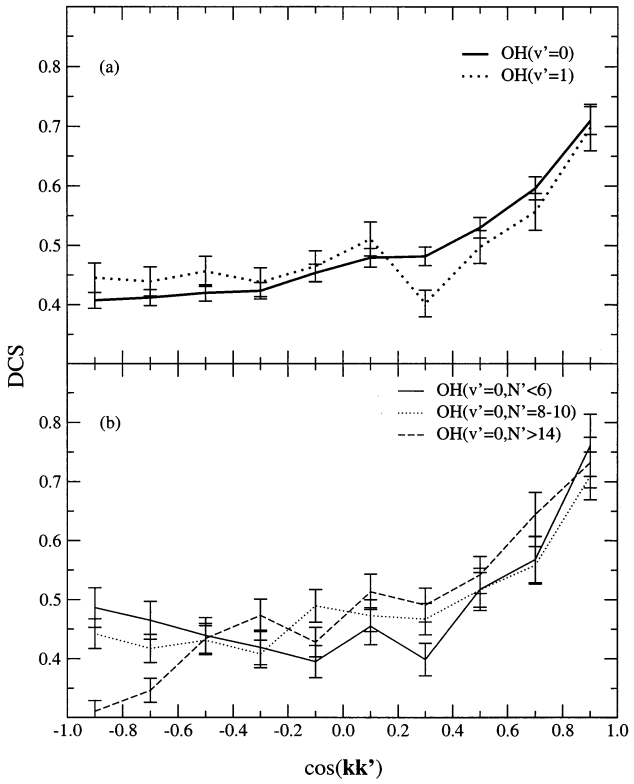

Figure 8. QCT angular distributions expressed in terms of normalized differential cross sections $[(2\pi/\sigma)(d\sigma/d\omega)]$ for the H + CO_2 → OH-(v',N') + CO reaction at E_T = 2.5 eV and using the PES derived in this work: (a) OH vibrational state-specific angular distributions; (b) OH rotational state-selected angular distributions.

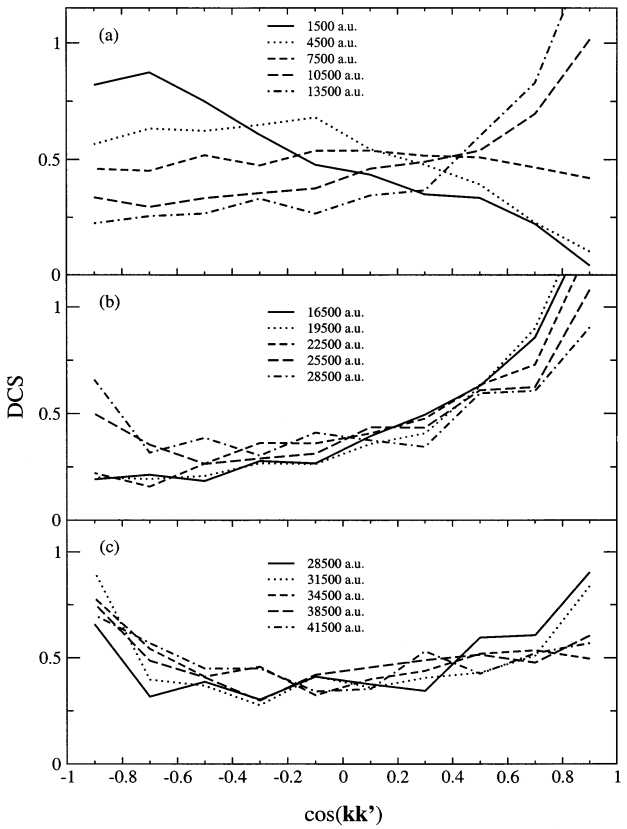

Figure 9. QCT angular distributions expressed in terms of normalized differential cross sections $[(2\pi/\sigma)(d\sigma/d\omega)]$ for different collision complex lifetime and the H + CO_2 → OH + CO reaction at E_T = 1.86 eV and using the PES derived in this work: (a) 0 au ≤ lifetime ≤ 15 000 au; (b) 15 000 au ≤ lifetime ≤ 30 000 au; (c) 27 000 au ≤ lifetime ≤ 43 000 au.

as the collision complex lifetime increases, so that at about 30 000 au, there is forward−backward symmetry. Panel c shows that the distribution becomes nearly isotropic for very long-lived complexes.

From these findings it is possible to formulate a model suitable to explain the angular distributions as a function of the collision complex lifetime. The scattering for complexes that live up to about 15 000 au agrees well with the osculating complex model first invoked by Casavecchia and co-workers[39] for the reverse reaction OH + CO → H + CO_2, such that the complex lifetime determines how much rotation has occurred and thereby the angular distribution. However, we see that the osculating complex is not a perfect model for longer-lived trajectories. One would expect that if the collision complex is allowed to rotate for one rotational period, strong backward scattering should be found. But we see that the scattering is never backward-dominated after 15 000 au. Instead the scattering becomes more and more forward−backward symmetric and then evolves into an isotropic distribution.

We find that this evolution in the angular distributions in Figure 9 results from dynamics of the HOCO complex that reflects the relative contributions of in-plane and out-of-plane angular motion. In particular, in-plane rotation leads to clear-cut correlations between initial impact parameter, complex lifetime, and angular distribution that are consistent with the osculating complex model, while out-of-plane rotation destroys these correlations and ultimately contributes to isotropic distributions. The relative importance of these two types of rotational motion depends on complex lifetime, as Coriolis coupling causes initial in-plane excitation to be converted to out-of-plane motion as the complex vibrates. To illustrate these points, we present in Figure 10 the opacity function at 1.86 eV for selected values of the collision complex lifetimes. In this figure we define forward scattering as referring to cos (**kk**′) > 0.45, backward scattering to cos (**kk**′) < −0.45, and sideways scattering as −0.45 < cos (**kk**′) < 0.45.

In panel a the global opacity function (i.e., including all complex lifetimes) is presented. Here we see the expected falloff of total reactivity with impact parameter, and we also find that the largest impact parameters preferentially lead to forward scattering, the smallest to backward scattering, and intermediate impact parameters to sideways scattering. However we also note that the forward, sideways, and backward peaks strongly overlap, meaning that the correlation of angular distribution and impact parameter is relatively weak. Figure 10b shows how these results are resolved for the 0−3000 au lifetime interval. Here we see a dominant backward peak that is associated with small impact parameters. This peak is well separated from the sideways peak at larger impact parameters, and there is also a small forward peak at the largest impact parameters. This behavior is very similar to what is often observed for direct reactions. Indeed, in examining individual collisions, we find that for the largest impact parameters the colliding H atom drags one of the O atoms forward after a very brief encounter that is analogous to stripping dynamics. Also, backward scattering is observed in collisions that despite very briefly forming complexes are analogous to a rebound mechanism.

Figure 10c shows that intermediate-lived complexes (15 000−18 000 au) lead to much larger forward scattering intensities, with general good correlation between impact parameter and scattering angle. Animation of trajectories reveals that in most collisions the incident H atom angular momentum is converted

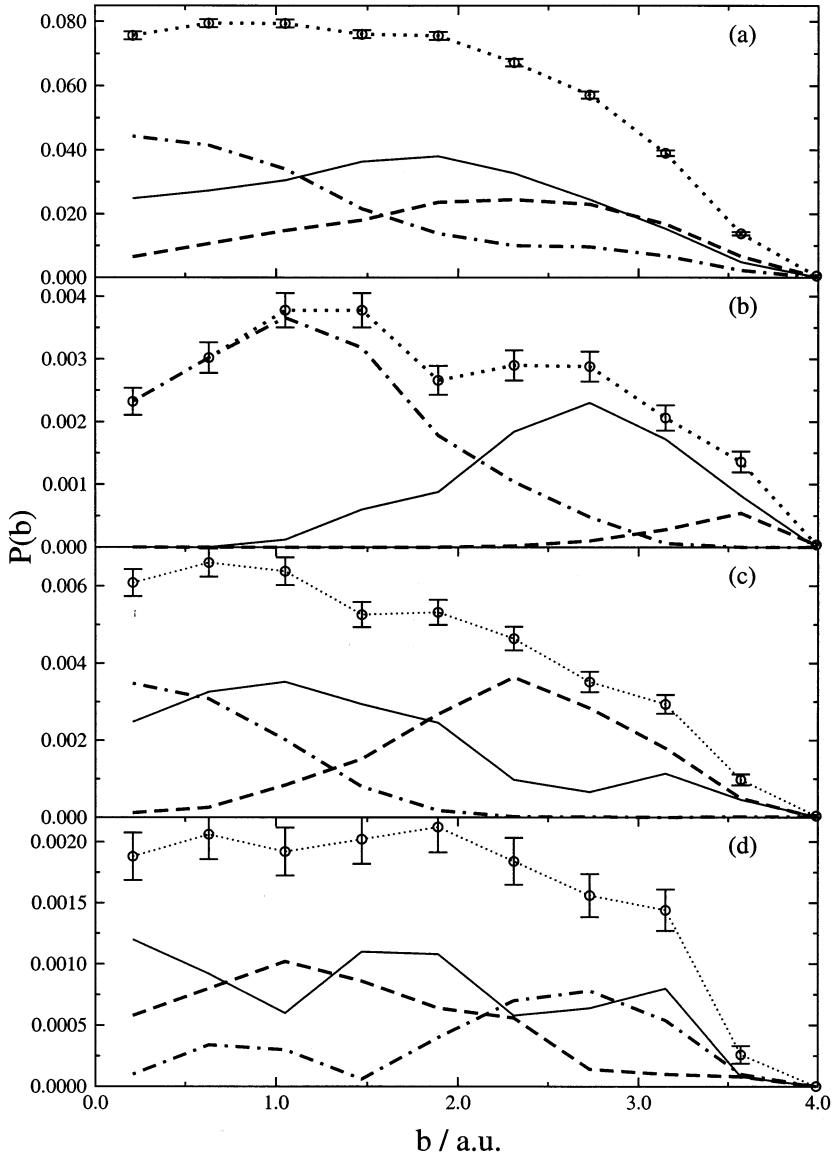

Figure 10. QCT opacity functions accounting for selected scattering regions for the H + CO_2 → OH + CO reaction at E_T = 1.86 eV and using the PES derived in this work: (a) Global opacity function; (b) 0 ≤ lifetime ≤ 3000 au; (c) 15 000 ≤ lifetime ≤ 18 000 au; (d) 35 000 ≤ lifetime ≤ 38 000 au. (○···○) Opacity function for the whole scattering space; (---) opacity functions of the trajectories scattered in the forward direction; (-·-) opacity functions of the trajectories scattered in the backward direction; (—) sideways scattering. See text for details.

into in-plane HOCO rotation, with the final scattering angle determined by the amount of rotation of the HOCO complex, and hence by the impact parameter. Note, however, that sideways scattering is possible for all impact parameters. This is due to the contribution of out-of-plane rotation for some of the HOCO complexes. Thus for large impact parameters, it is possible to convert some of the initial orbital angular momentum into out-of-plane rotational motion that no longer gives a clean correlation with forward scattering.

Figure 10d shows that long-lived complexes (35 000−38 000 au) produce isotropic scattering wherein the forward, backward, and sideways components of the angular distribution have comparable cross sections. The correlation between initial impact parameter and final scattering angle is weaker than in the earlier panels, but it shows that forward scattering comes primarily from small impact parameters (which would produce slowly rotating complexes that would only have executed half a rotation during the chosen time window) while backward scattering comes from large impact parameter collisions (which produce complexes that undergo a complete rotation during the chosen time). The weaker correlation between impact parameter and scattering angle reflects the increasing importance of out-of-plane rotation.

As a point of reference, we note that, at 1.86 eV, the orbital angular momentum associated with an initial impact parameter b is equal to 11b, while the initial rotational angular momentum of the CO_2 is 15, so CO_2 rotation will play a role in determining the total angular momentum of the complex for impact parameters below about 1.5 au. This suggests that the correlations between initial impact parameter and scattering angle could be significantly altered if the CO_2 were more highly rotationally excited or rotationally aligned. To verify this, we have carried out calculations at 1.86 eV with $j(CO_2)$ = 40. The resulting angular distribution has a very slightly increased intensity in the peak of the extreme backward region, but the global distribution is still forward-biased. To illustrate this, the average scattering angle increases from 84.4 ± 0.6 for $j(CO_2)$ = 15 to 86.8 ± 0.9 for $j(CO_2)$ = 40, and the forward/backward ratios (cross section of the trajectories scattered in the forward hemisphere over that of those scattered in the backward one)

are 1.38 and 1.18, respectively. Study of collision complex lifetime-resolved scattering distributions under these conditions reveals that the scattering in the 20 000−30 000 au interval is less forward than for $j(CO_2) = 15$, thereby giving the slightly more backward global distribution. Animation of trajectories indicates that in-plane complex rotation is faster for the higher initial CO_2 rotation, as expected, so complexes that, for $j(CO_2) = 15$, were able to exert only a half-turn now successfully give a full turn and provide enhanced backward scattering.

IV. Concluding Remarks

We have undertaken an extensive dynamics study of the complex-forming bimolecular reaction H + CO_2 → OH + CO at kinetic energies that correspond to most of the experiments that have been done for this system. To do so, we have employed the previously reported BS analytical potential energy surface[14] along with two surfaces that provide important improvements to BS. In the BSH surface, we have only changed the exit channel portion of BS that takes the system over the HOCO saddle point to OH + CO. This has been accomplished by constructing a local six-dimensional function with a three-dimensional spline fit to a grid of ab initio points and adding semiempirical functions for the remaining degrees of freedom. In addition, the functional dependence of the BS potential has been modified to smooth out singularities in the derivatives. In the LTSH surface, the energies of the various stationary points that are encountered prior to the exit channel region have been adjusted so as to reproduce recent high-level ab initio estimates.

We find that these modifications to the BS surface lead to a much better match with the experimental measurements, with the more important factor being the modified exit channel potential (narrower reaction path with more bent transition state) that is contained in both BSH and LTSH. In particular, there is a larger energy release to product CO rotation and a corresponding decrease in translational excitation on both BSH or LTSH, which is in agreement with global and OH state-resolved experimental determinations. Experimental OH rotational state-specific angular distributions are also well described by these two surfaces, particularly by the LTSH PES.

Because it is now possible to integrate literally millions of trajectories on these new surfaces, we have been able to address several mechanistic issues concerning the H + CO_2 reaction that have not been addressed earlier, and which in some cases represent surprising results when compared with simpler models that have been used previously to understand this reaction. In particular, we find that the product energy distributions are essentially independent of complex lifetime. This implies that energy transfer between modes of the complex does not influence these distributions very much. Instead it is the shape of the potential in the exit channel that controls these distributions. In contrast to this, the angular distributions are very sensitive to the complex lifetime. Here the osculating model provides a reasonable picture of the evolution of the system for roughly the first half rotation of the HOCO complex, with backward scattering being dominant at very short times and then forward scattering after half a rotation. After that we find that the osculating complex model is less useful, as the angular distribution evolves into a forward−backward symmetric distribution after one rotational period and ultimately into an isotropic distribution for long HOCO lifetimes. We find that this behavior may be understood in terms of the relative contributions of in-plane and out-of-plane rotation of the HOCO complex, with in-plane motions showing good correlation between initial impact parameter and final scattering angle, while out-of-plane motions, which grow in importance as the complex evolves, hinder the correlation between complex lifetime and angular distribution. In a forthcoming paper the effects of these surfaces on the dynamics of the reverse reaction OH + CO → H + CO_2 will be shown. In addition, there are a number of interesting phenomena yet to be discussed for the title reaction, including the importance of nonadiabatic effects and the description of OH rotational polarization.

Acknowledgment. This research was supported by NSF Grant CHE-0131998, by the Spanish Ministry of Education and Culture (M.E.C.) through Projects DGES PB98-1209-C02-01 and -02, and by the "Generalitat de Catalunya" (Autonomous Government), Project 2000SGR 00016. The Centre de Supercomputació i Comunicacions de Catalunya, (C^4(CESCA/CEPBA)) is also acknowledged for computation time made available. L.B.H. was supported by the U.S. Department of Energy, Office of Basic Energy Sciences, Division of Chemical Sciences, Geosciences, and Biosciences under DOE Contract W-31-109-ENG-38.

References and Notes

(1) Miller, J. A.; Kee, R. J.; Westbrook, C. K. *Annu. Rev. Phys. Chem.* **1990**, *41*, 345.

(2) McCormack, D. A.; Kroes, G.-J. *Chem. Phys. Lett.* **2002**, *352*, 281.

(3) (a) Zewail, A. H. *Science* **1988**, *242*, 1645. (b) Wittig, C.; Sharpe, S.; Beaudet, R. A. *Acc. Chem. Res.* **1988**, *21*, 341. (c) Flynn, G. W. *Science* **1989**, *246*, 1009.

(4) (a) Chen, Y.; Hoffmann, G.; Oh, D.; Wittig, C. *Chem. Phys. Lett.* **1989**, *159*, 426. (b) Hoffmann, G.; Oh, D.; Chen, Y.; Engel, Y. M.; Wittig, C. *Isr. J. Chem.* **1990**, *30*, 115. (c) Wittig, C.; Engel, Y. M.; Levine, R. D. *Chem. Phys. Lett.* **1988**, *153*, 411.

(5) (a) Kleinermanns, K.; Wolfrum, J. *Chem. Phys. Lett.* **1984**, *104*, 157. (b) Kleinermanns, K.; Linnebach, E.; Wolfrum, J. *J. Phys. Chem.* **1985**, *89*, 2525. (c) Jacobs, A.; Wahl, M.; Weller, R.; Wolfrum, J. *Chem. Phys. Lett.* **1989**, *158*, 161. (d) Jacobs, A.; Volpp, H.-R.; Wolfrum, J. *Chem. Phys. Lett.* **1994**, *218*, 51.

(6) Rice, J. K.; Baronavski, A. P. *J. Chem. Phys.* **1991**, *94*, 1006.

(7) Nickolaisen, S. L.; Cartland, H. E.; Wittig, C. *J. Chem. Phys.* **1992**, *96*, 4378.

(8) (a) Brouard, M.; Lambert, H. M.; Rayner, S. P.; Simons, J. P. *Mol. Phys.* **1996**, *89*, 493. (b) Brouard, M.; Hughes, D. W.; Kalogerakis, K. S.; Simons, J. P. *J. Phys. Chem. A* **1998**, *102*, 9559.

(9) Brouard, M.; Hughes, D. W.; Kalogerakis, K. S.; Simons, J. P. *J. Chem. Phys.* **2000**, *112*, 4557.

(10) Brouard, M.; Burak, I.; Hughes, D. W.; Kalogerakis, K. S.; Simons, J. P.; Stavros, V. *J. Chem. Phys.* **2000**, *113*, 3173.

(11) Schatz, G. C.; Fitzcharles, M. S.; Harding, L. B. *Faraday Discuss. Chem. Soc.* **1987**, *84*, 359.

(12) Kudla, K.; Schatz, G. C.; Wagner, A. F. *J. Chem. Phys.* **1991**, *95*, 1635.

(13) Kudla, K.; Schatz, G. C. *J. Phys. Chem.* **1991**, *95*, 8267.

(14) Bradley, K. S.; Schatz, G. C. *J. Phys. Chem.* **1997**, *106*, 8864.

(15) Zhu, D. S.; Diau, E. G. W.; Lin, M. C.; Mebel, A. M. *J. Phys. Chem. A* **2001**, *105*, 11249.

(16) Duncan, T. V.; Miller, C. E. *J. Chem. Phys.* **2000**, *113*, 5138.

(17) Yu, H.-G.; Muckerman, J. T.; Sears, T. J. *Chem. Phys. Lett.* **2001**, *349*, 547.

(18) (a) Lester, M. I.; Pond, B. V.; Anderson, D. T.; Harding, L. B.; Wagner, A. F. *J. Chem. Phys.* **2000**, *113*, 9889. (b) Lester, M. I.; Pond, B. V.; Marshall, M. D.; Anderson, D. T.; Harding, L. B.; Wagner, A. F. *Faraday Discuss.* **2001**, *118*, 373.

(19) Kudla, K.; Koures, A. G.; Harding, L. B.; Schatz, G. C. *J. Chem. Phys.* **1992**, *96*, 7465.

(20) Wu, G.-S.; Schatz, G. C.; Lendvay, G.; Fang, D.-C.; Harding, L. B. *J. Chem. Phys.* **2000**, *113*, 3150.

(21) Knowles, P. J.; Hampel, C.; Werner, H.-J. *J. Chem. Phys.* **1993**, *99*, 5219.

(22) Dunning, T. H., Jr. *J. Chem. Phys.* **1989**, *90*, 1007.

(23) Kendall, R. A.; Dunning, T. H., Jr.; Harrison, R. J. *J. Chem. Phys.* **1992**, *96*, 6796.

(24) Woon, D. E.; Dunning, T. H., Jr. *J. Chem. Phys.* **1993**, *98*, 1358.

(25) MOLPRO is a package of ab initio programs written by H.-J. Werner and P. J. Knowles, with contributions from J. Almlof, R. D. Amos, A. Berning, D. L. Cooper, M. J. O. Deegan, A. J. Dobbyn, F. Eckert, S. T.

Elbert, C. Hampel, R. Lindh, A. W. Lloyd, W. Meyer, A. Nicklass, K.Peterson, R. Pitzer, A. J. Stone, P. R. Taylor, M. E. Mura, P. Pulay, M. Schutz, H. Stoll, and T. Thorsteinsson.

(26) Sathyamurthy, N.; Raff, L. M. *J. Chem. Phys.* **1975**, *63*, 464.

(27) LTSH PES: M. J. Lakin, D. Troya, G. C. Schatz, and L. B. Harding, manuscript in preparation.

(28) Troya, D.; Baños, I.; González, M.; Wu, G.-S.; ter Horst, M. A.; Schatz, G. C. *J. Chem. Phys.* **2000**, *113*, 6253.

(29) Troya, D.; González, M.; Wu, G.-S.; Schatz, G. C. *J. Phys. Chem. A* **2001**, *105*, 2285.

(30) Troya, D.; González, M.; Schatz, G. C. *J. Chem. Phys.* **2001**, *114*, 8397.

(31) Troya, D.; Lendvay, G.; González, M.; Schatz, G. C. *Chem. Phys. Lett.* **2001**, *343*, 420.

(32) Schatz, G. C. *Comput. Phys. Commun.* **1988**, *51*, 135.

(33) Schatz, G. C.; ter Host, M. A.; Takayanagi, T. In *Computational Methods for Polyatomic Bimolecular Reactions.*; Thompson, D. L., Ed.; World Scientific: Singapore, 1998.

(34) Bradley, K. S.; Schatz, G. C. *J. Chem. Phys.* **1998**, *108*, 7994.

(35) Adelman, D. E.; Filseth, S. V.; Zare, R. N. *J. Chem. Phys.* **1993**, *98*, 4636.

(36) Brouard, M.; Burak, I.; Joseph, D. M.; Markillie, G. A. J.; Minayev, D.; O'Keefe, P.; Vallence, C. *J. Chem. Phys.* **2001**, *114*, 6690.

(37) Woodruff, S. B.; Thompson, D. L. *J. Chem. Phys.* **1979**, *71*, 376.

(38) Germann, G. J.; Huh, Y. D., Valentini, J. J. *J. Chem. Phys* **1992**, *96*, 1957.

(39) (a) Alagia, M.; Balucani, N.; Casavecchia, P.; Stranges, D.; Volpi, G. G. *J. Chem. Phys.* **1993**, *98*, 8341. (b) Casavecchia, P.; Balucani, N.; Volpi, G. G. In *Research in Chemical Kinetics*; Compton, R. G., Hancock, G., Eds.; Elsevier: Amsterdam, 1993; Vol. I, p 1.